Journal of Sound and Vibration 331 (2012) 117–137

Contents lists available at SciVerse ScienceDirect

Journal of Sound and Vibration

journal homepage: www.elsevier.com/locate/jsvi

# A moving medium formulation for prediction of propeller noise at incidence

Ghader Ghorbaniasl *, Chris Lacor

*Vrije Universiteit Brussel, Pleinlaan 2, 1050 Brussels, Belgium*

ARTICLE INFO

*Article history:*
Received 17 September 2010
Received in revised form
10 May 2011
Accepted 17 August 2011
Handling Editor: P. Joseph
Available online 16 September 2011

ABSTRACT

This paper presents a time domain formulation for the sound field radiated by moving bodies in a uniform steady flow with arbitrary orientation. The aim is to provide a formulation for prediction of noise from body so that effects of crossflow on a propeller can be modeled in the time domain. An established theory of noise generation by a moving source is combined with the moving medium Green's function for derivation of the formulation. A formula with Doppler factor is developed because it is more easily interpreted and is more helpful in examining the physic of systems. Based on the technique presented, the source of asymmetry of the sound field can be explained in terms of physics of a moving source. It is shown that the derived formulation can be interpreted as an extension of formulation 1 and 1A of Farassat based on the Ffowcs Williams and Hawkings (FW–H) equation for moving medium problems. Computational results for a stationary monopole and dipole point source in moving medium, a rotating point force in crossflow, a model of helicopter blade at incidence and a propeller case with subsonic tips at incidence verify the formulation.



## 1. Introduction

Excessive aircraft noise nuisance is one of the most important problems in today's technological society. It has become necessary to develop new tools, including theoretical, computational and experimental approaches that will allow the robust and accurate prediction of sound levels from aircraft airframes and engines. Therefore, a relatively new discipline, Computational Aeroacoustics (CAA), has emerged. Computational Aeroacoustics (CAA) poses significant challenges for researchers in the accurate prediction of the acoustic fluctuations and their correct propagation to the far field.

The prediction of noise from an aerodynamic source is a question of estimating noise generated from a solid body, a flow or interactions between flow and solid. Aeroacoustics combines the discipline of fluid mechanics with classical acoustics, making problems complicated. In aeroacoustics, problems are divided into three categories. The first category consists of an observer fixed in a stationary ambient medium and of a source, which can be either in motion or at rest. The second category is referred to as 'moving observer', dealing with problems where the observer is in motion as well as the source so that the source and observer move relative to a fixed reference frame and, perhaps, relative to each other. In the third category referred to as 'moving medium', the sound is received by a stationary observer in a moving medium. The problem of noise generated by a propeller in the cabin of an aircraft or on its fuselage can be considered either as a 'moving observer' or a 'moving medium' problem.

* Corresponding author. Tel.: +3226292396; fax: +3226292880.
*E-mail address:* ghader.ghorbaniasl@vub.ac.be (G. Ghorbaniasl).

0022-460X/$ - see front matter © 2011 Elsevier Ltd. All rights reserved.
doi:10.1016/j.jsv.2011.08.018

**Nomenclature**

| | |
|---|---|
| $c_0$ | speed of sound |
| $f$ | data surface |
| $g$ | retarded time function |
| $G$ | Green's function |
| $H$ | Heaviside function |
| $M_i$ | source Mach number vector |
| $M_{\infty i}$ | inflow Mach number vector |
| $\hat{n}_i$ | surface unit normal |
| $p$ | pressure |
| $p'$ | acoustic pressure fluctuation |
| $P_{ij}$ | compressive stress tensor |
| $r$ | distance between observer and source |
| $R,R^*$ | acoustic radii |
| $\tilde{R}_i$ | $\partial R/\partial x_i$ |
| $\tilde{R}^*_i$ | $\partial R^*/\partial x_i$ |
| $S$ | data surface area |
| $t$ | observer time |
| $T_{ij}$ | Lighthill stress tensor |
| $u_i$ | flow velocity |
| $v_i$ | data surface velocity |
| $x_i$ | observer position |
| $y_i$ | source position |

*Greek letters*

| | |
|---|---|
| $\alpha$ | angle of attack |
| $\beta$ | angle of observer |
| $\delta$ | Dirac delta function |
| $\delta_{ij}$ | Kronecker delta |
| $\rho$ | density |
| $\rho_0$ | undisturbed flow density |
| $\rho'$ | acoustic density fluctuation |
| $\sigma_{ij}$ | viscous stress tensor |
| $\tau$ | emission time variable |

The Ffowcs Williams and Hawkings (FW–H) equation [1] is a standard approach for problems of the first two categories. Farassat [2–4] has developed several time domain formulations for the solution of the FW–H equation. In particular, the formulations 1 and 1A provide a solution for the monopole and dipole subsonic sources for a given geometry, displacement and aerodynamic loading of moving bodies. These formulations are the most widely used time domain techniques for airframe noise applications. They have typically been applied to the data surface to coincide with solid bodies, but are still applicable when the surface is off the body and permeable.

Moving medium problems can be analyzed in two distinct approaches. First, the moving medium problem is transformed into an equivalent problem of the second category, where the formulations of Farassat are used. This approach does not explicitly take into account the presence of the mean flow. An alternative approach for problems of the third category is to use a moving medium method, which usually is useful. This approach explicitly takes into account the presence of the mean flow effect. The present paper deals with the moving medium approach.

The problem of a propeller operating at some angle to the flight direction is linked to the change of the radiated noise level. The effect of angle of attack can be equivalent to an unsteady acoustic source, resulting in generation of more efficient radiation modes. These radiation modes themselves are modified, causing further efficiency increase (see Hanson [5]). The main objective of this paper is to develop a time domain moving medium formulation, which takes into account the mean flow influence and the aerodynamic and acoustic effects of incidence. A formula with Doppler factor is derived because it is more easily interpreted and is more helpful in examining the physics of systems. The time domain formulation presented here follows the approach used by Hanson and Paryzch [6] and Hanson [5] to develop exact frequency domain formulations, which include the convective effect at an angle of attack.

Based on this approach, the source of asymmetry of the sound field can be explained in terms of the physics of a moving source rather than in terms of spinning modes.

One can use the technique presented to give a formula, which contains no Doppler factor to ease the prediction of the noise from the translating supersonic propellers. Wells and Han [7] have recently developed a formulation for supersonic propellers with an axial inflow. Their technique does not deal with the problem of a propeller at incidence. They have observed that the moving medium method greatly reduces the computational effort for the supersonic propeller (one-sixth of the computational time of the moving observer method). However, derivation of the formulation for supersonic propellers at incidence is not inside the scope of the current paper, but will be the purpose of future work.

The formulation to be developed in this paper will be based on a moving medium, subsonic propeller technique taking into account the aerodynamic and acoustic effect of incidence. It will be a moving medium version of formulations 1 and 1A of Farassat, showing explicitly the effect of incidence on the Doppler amplification of the radiated noise. The formulation derived allows the convective effect on propeller noise to be decoupled from the rotational and unsteady loading effects. The remarkable feature of the formulation is that it provides a way of examining the physics of the problem and enables us to process asymmetric inflow effects.

The formulation derived will be tested through five test cases. The test cases are as follows: a stationary monopole and dipole point source in a moving medium with different orientations, a rotation dipole point source in crossflow, a model of a helicopter blade operating at incidence, and a the consistency test known as Isom thickness noise for a propeller with subsonic tips at incidence. Computational results verify formulations, indicating that the time domain moving medium method predicts the noise radiated from moving bodies at incidence accurately. It is shown that developed formulations are useful and can be coded for efficient prediction of sound field generated by propellers at incidence.

The remainder of the paper describes the time domain moving medium method in enough detail to show the similarities and differences between the convective and non-convective wave equations. A discussion of numerical implementation follows. Finally, five test cases are used to verify the method, demonstrating the utility and efficiency of the scheme.

## 2. Radiated sound from a moving body

The source terms in the wave equation are handled by generalized functions used by Farassat [8,9]. This technique is used in three dimensions, in dealing with geometrical relationships. A data surface in space is defined by a function $f(\vec{x},t)$, bounding the considered flow domain around the body (see Fig. 1),

$$f(\vec{x},t)\begin{cases} <0 & \text{inside the boundary} \\ =0 & \text{on the boundary} \\ >0 & \text{outside the boundary} \end{cases} \tag{1}$$

In accordance with the convention of Farassat [9] we assume that

$$|\vec{\nabla} f| = 1 \tag{2}$$

so that $\partial f/\partial x_i = \hat{n}_i$ with $i = 1,2,3$ is the local outer normal of the data surface. The surface is assumed to be smooth, without discontinuities. The Heaviside function of $f(\vec{x},t)$ is defined as follows:

$$H(f) = \begin{cases} 1 & f(\vec{x},t) > 0 \\ 0 & f(\vec{x},t) < 0 \end{cases} \tag{3}$$

Dirac's delta function of $f(\vec{x},t)$ is described by

$$\delta(f) = \frac{\partial H(f)}{\partial f} = \begin{cases} 1 & f(\vec{x},t) = 0 \\ 0 & f(\vec{x},t) \neq 0 \end{cases} \tag{4}$$

Using Eq. (4), the spatial derivate of the Heaviside function can be expressed by

$$\frac{\partial H(f)}{\partial x_i} = \frac{\partial H(f)}{\partial f}\frac{\partial f}{\partial x_i} = \delta(f)\hat{n}_i \tag{5}$$

For a data surface moving with velocity of the body $v_i$, the function $f$ satisfies the following equation:

$$\mathrm{d}f(x_i,t) = \frac{\partial f}{\partial t}\mathrm{d}t + \frac{\partial f}{\partial x_i}\mathrm{d}x_i = 0 \tag{6}$$

or

$$\frac{\partial f}{\partial t} = -v_i\frac{\partial f}{\partial x_i} \tag{7}$$

Therefore, using (4) and (7) can give the time derivative of the Heaviside function as follows:

$$\frac{\partial H(f)}{\partial t} = \frac{\partial H(f)}{\partial f}\frac{\partial f}{\partial t} = -v_i\hat{n}_i\delta(f) \tag{8}$$

Through the above generalized functions, the basic equations of aerodynamics can be transformed to the wave equation containing the source terms. The starting point can be continuity equation modified by multiplication by the Heaviside

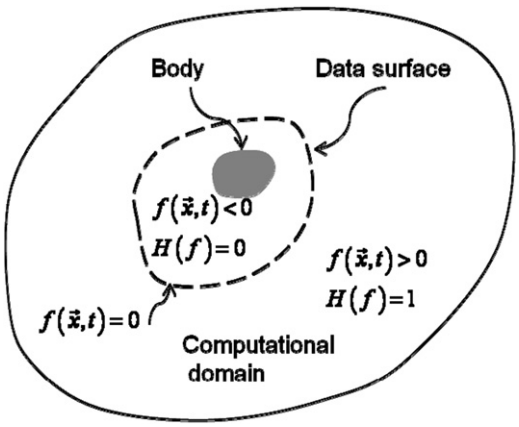


**Fig. 1.** Description of data surface in a computational domain.

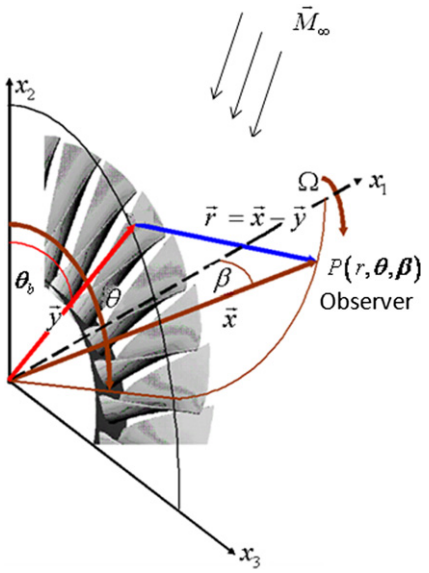


**Fig. 2.** Flow over a source and an observer.

function, which defines the data surface of interest. Multiplying by the Heaviside function simply means that the equation is valid only outside of the data surface.

First, assume that the coordinates $\vec{x}'$ is fixed to the ground, and the coordinates $\vec{x}$ moves with the observer in the negative directions of the coordinates $\vec{x}'$. This problem is equivalent to that of flow over the stationary observer blowing in the positive directions of $\vec{x}'$, where the source moves relative to the observer (see Fig. 2). In the two systems of coordinates, the spatial derivatives will be unchanged, but the time derivatives will be obtained as

$$\frac{D}{Dt} = \frac{\partial}{\partial t} + U_{\infty i}\frac{\partial}{\partial x_i} \tag{9}$$

where $U_{\infty i}$ is the $i$th component of the mean flow velocity. Therefore, the quantity equation for space outside the surface is, replacing $\partial/\partial t$ with $D/Dt$,

$$H(f)\left[\frac{D}{Dt}(\rho-\rho_0)+\frac{\partial}{\partial x_i}(\rho u_i)\right] = 0 \tag{10}$$

where is the density of fluid, $u_i$ denotes the fluid velocity and $\rho_0$ denotes the fluid density at rest. Using the rule for differentiation of products, Eq. (10) is rewritten as

$$\frac{D}{Dt}\left[(\rho-\rho_0)H(f)\right]-(\rho-\rho_0)\frac{DH(f)}{Dt}+\frac{\partial}{\partial x_i}\left[\rho u_i H(f)\right]-\rho u_i\frac{\partial H(f)}{\partial x_i} = 0 \tag{11}$$

The second and fourth terms in Eq. (11) are moved to the right-hand side and the equation is simplified as follows using relations (5) and (8),

$$\frac{D}{Dt}\left[(\rho-\rho_0)H(f)\right]+\frac{\partial}{\partial x_i}\left[\rho u_i H(f)\right] = \left[\rho_0(v_i-U_{\infty i})\hat{n}_i+\rho(v)\hat{n}_i\right]\delta(f) \tag{12}$$

Let

$$\begin{aligned} Q &= \rho(u_i+U_{\infty i}-v_i)\hat{n}_i+\rho_0(v_i-U_{\infty i})\hat{n}_i \\ &= \rho(u_n+U_{\infty n}-v_n)+\rho_0(v_n-U_{\infty n}) \end{aligned} \tag{13}$$

where subscript $n$ denotes the local normal term of the data surface. The following continuity equation for the function $(\rho-\rho_0)H(f)$ is given by

$$\frac{D}{Dt}\left[(\rho-\rho_0)H(f)\right]+\frac{\partial}{\partial x_i}\left[\rho u_i H(f)\right] = Q\delta(f) \tag{14}$$

This function is equal to the density fluctuation outside the boundary surface, and equal to 0 inside of it. The source term $Q$ exists on $S$, and accounts for all boundary effects.

The same methodology is applied to the momentum equation. The nonlinear momentum equation can be written in a similar fashion as

$$H(f)\left\{\frac{D}{Dt}(\rho u_i)+\frac{\partial}{\partial x_j}(\rho u_i u_j)+\frac{\partial}{\partial x_j}\left[(p\delta_{ij}-\sigma_{ij})\right]\right\}=0 \tag{15}$$

One has

$$\begin{aligned}&\frac{D}{Dt}\left[\rho u_i H(f)\right]+\frac{\partial}{\partial x_j}\left[\rho u_i u_j H(f)\right]+\frac{\partial}{\partial x_j}\left[(p\delta_{ij}-\sigma_{ij})H(f)\right]\\&=\rho u_i\left(\frac{\partial H(f)}{\partial t}+U_{\infty j}\frac{\partial H(f)}{\partial x_j}\right)+\rho u_i u_j\frac{\partial H(f)}{\partial x_j}+p\delta_{ij}\frac{\partial H(f)}{\partial x_j}-\sigma_{ij}\frac{\partial H(f)}{\partial x_j}\end{aligned} \tag{16}$$

The right-hand side of Eq. (16) can be simplified as follows:

$$\begin{aligned}&\frac{D}{Dt}\left[\rho u_i H(f)\right]+\frac{\partial}{\partial x_j}\left[\rho u_i u_j H(f)\right]+\frac{\partial}{\partial x_j}\left[(p\delta_{ij}-\sigma_{ij})H(f)\right]\\&=\rho u_i(u_j+U_{\infty j}-v_j)\hat{n}_j\delta(u_j+U_{\infty j}-v_j)+(p\delta_{ij}-\sigma_{ij})\hat{n}_j\delta(f)\end{aligned} \tag{17}$$

Let

$$L_i=[P_{ij}+\rho u_i(u_j+U_{\infty j}-v_j)]\hat{n}_j=P_{ij}\hat{n}_j+\rho u_i(u_n+U_{\infty n}-v_n) \tag{18}$$

The term $P_{ij}$ denotes the compressive stress tensor

$$P_{ij}=(p-p_0)\delta_{ij}-\sigma_{ij} \tag{19}$$

where $p_0$ denotes the fluid pressure at rest. The momentum equation for the generalized function $\rho u_i H(f)$ is given by

$$\frac{D}{Dt}\left[\rho u_i H(f)\right]+\frac{\partial}{\partial x_j}\left[\rho u_i u_j H(f)\right]+\frac{\partial}{\partial x_j}\left[(p\delta_{ij}-\sigma_{ij})H(f)\right]=L_i\delta(f) \tag{20}$$

In this equation, the source term $L_i$ accounts for the flux of momentum across the surface. In this source term, the constant pressure $p_0$ is inserted for convenience. The original continuity and momentum equations are valid only in the space occupied by the fluid, whereas Eqs. (14) and (20) are valid throughout all space.

Taking the time derivative of the continuity Eq. (14) and subtracting the divergence of the momentum Eq. (20) gives

$$\begin{aligned}&\frac{D^2}{Dt^2}\left[(\rho-\rho_0)H(f)\right]+\frac{D}{Dt}\left\{\frac{\partial}{\partial x_i}\left[\rho u_i H(f)\right]\right\}-\frac{\partial}{\partial x_i}\left\{\frac{D}{Dt}\left[\rho u_i H(f)\right]\right\}-\frac{\partial^2}{\partial x_i\partial x_j}\left[\rho u_i u_j H(f)\right]\\&-\frac{\partial^2}{\partial x_i\partial x_j}\left[(p\delta_{ij}-\sigma_{ij})H(f)\right]=\frac{D}{Dt}\left[Q\delta(f)\right]-\frac{\partial}{\partial x_i}L_i\delta(f)\end{aligned} \tag{21}$$

or

$$\frac{D^2}{Dt^2}\left[(\rho-\rho_0)H(f)\right]-\frac{\partial^2}{\partial x_i\partial x_j}\left[\rho\, u_i u_j H(f)\right]=\frac{\partial^2}{\partial x_i\partial x_j}(p\delta_{ij}-\sigma_{ij})-\frac{\partial}{\partial x_i}\left[L_i\delta(f)\right]+\frac{D}{Dt}\left[Q\delta(f)\right] \tag{22}$$

Adding and subtracting the term $c_0^2\ \partial^2/\partial x_i\partial x_i[(\rho-\rho_0)H(f)]$ and yield a wave equation with source terms accounting for the boundary effect,

$$\left[\frac{D^2}{Dt^2}-c_0^2\frac{\partial^2}{\partial x_i\partial x_i}\right]\left\{\rho'(\vec{x},t)H(f)\right\}=\frac{\partial^2}{\partial x_i\partial x_j}\left[T_{ij}H(f)\right]-\frac{\partial}{\partial x_i}\left[L_i\delta(f)\right]+\frac{D}{Dt}\left[Q\delta(f)\right] \tag{23}$$

where $\rho'(\vec{x},t)=\rho(\vec{x},t)-\rho_0$ and $c_0$ the speed of sound in the unbounded space. Note that an equivalent form of Eq. (23) is obtained for the acoustic pressure field $p'(\vec{x},t)=c_0^2\rho'(\vec{x},t)$ through the relation

$$\left[\frac{1}{c_0^2}\frac{D^2}{Dt^2}-\nabla^2\right]\left\{p'(\vec{x},t)H(f)\right\}=\underbrace{\frac{\partial^2}{\partial x_i\partial x_j}\left[T_{ij}H(f)\right]}_{quadrupole}-\underbrace{\frac{\partial}{\partial x_i}\left[L_i\delta(f)\right]}_{loading}+\underbrace{\frac{D}{Dt}\left[Q\delta(f)\right]}_{thickness} \tag{24}$$

with

$$\begin{aligned}T_{ij}&=\rho u_i u_j+[(p-p_0)-c_0^2(\rho-\rho_0)]\delta_{ij}-\sigma_{ij}\\L_i&=\rho u_i[u_n-(v_n-U_{\infty n})]+P_{ij}\hat{n}_j\\Q&=\rho[u_n-(v_n-U_{\infty n})]+\rho_0(v_n-U_{\infty n})\end{aligned} \tag{25}$$

where the flow quantities are given in coordinates fixed to the undisturbed medium. Note that in Eq. (24) that the thickness and loading source terms are surface distributions of sources indicated by the presence of the Dirac delta function $\delta(f)$. The quadrupole source, on the other hand, is a volume distribution of sources. The quadrupole source accounts for the nonlinearities due to the turbulence, the local sound speed variation and the flow velocity near the blade, for instance the wakes.

As can be seen, the thickness and loading noise sources are slightly changed in comparison with the classical FW–H method. The quadrupole source remains in the same form as in the classical FW–H approach. The changes in the thickness and loading noise sources are related to the velocity of the moving body. In the moving medium technique, the loading and thickness noise source expressions consist in the relative velocity of the body to the moving medium, i.e. $v_n - U_{\infty n}$. For the classical FW–H approach, the loading and thickness source expressions contain the absolute velocity of the body, i.e. $v_n$. It indicates that when no mean flow exists the term $v_n - U_{\infty n}$ reduces to $v_n$, as expected for the case of a medium at rest.

If the data surface is taken as the moving body surface the fluid velocity on the surface is equal to the relative velocity of the body, i.e. $u_n = v_n - U_{\infty n}$. Therefore, the source term $Q$ is given by

$$Q = \rho_0 (v_n - U_{\infty n}) \tag{26}$$

and $L_i$ reduces to the force exerted by the body on the fluid

$$L_i = P_{ij} \hat{n}_j \tag{27}$$

## 3. Solution methods

The general form of the forced wave equation is given by

$$\left[ \frac{1}{c_0^2} \frac{D^2}{Dt^2} - \nabla^2 \right] \left\{ p'(\vec{x}, t) \right\} = q(\vec{x}, t) \tag{28}$$

A key feature of the wave equation obtained for a solid body in a flow is that it is an inhomogeneous wave equation for the external flow problem, embedded in unbounded space. Hence, an integral representation of the solution can be readily found using the free-space Green's function. Using Green's theorem we can construct an integral equation, which combines the effect of sources, propagation, boundary conditions and initial conditions in a simple formula. The Green's function $G(\vec{x}, t; \vec{y}, \tau)$ is the pulse response of the wave equation

$$\left( \frac{1}{c_0^2} \frac{D^2}{Dt^2} - \nabla^2 \right) G = \delta(\vec{x} - \vec{y}) \delta(t - \tau) \tag{29}$$

where $\delta(\vec{x} - \vec{y}) = \delta(x_1 - y_1)\delta(x_2 - y_2)\delta(x_3 - y_3)$. The pulse $\delta(\vec{x} - \vec{y})\delta(t - \tau)$ is released at the source point $\vec{y}$ at time $\tau$ and $G$ is measured at the observation point $\vec{x}$ at time $t$. Given the forced wave equation in a moving medium, the source distribution can be thought of as a distribution of impulsive point sources such that

$$q(\vec{x}, t) = \int_{-\infty}^{t} \int_{-\infty}^{\infty} q(\vec{y}, \tau) \delta(\vec{x} - \vec{y}) \delta(t - \tau) d^3 \vec{y} \, \mathrm{d}\tau \tag{30}$$

The addition of the individual point source contributions leads to the total representation for the fluctuating pressure at point $\vec{x}$ in the form

$$p'(\vec{x}, t) = \int_{-\infty}^{t} \int_{-\infty}^{\infty} q(\vec{y}, \tau) G(\vec{x}, t; \vec{y}, \tau) d^3 \vec{y} \, \mathrm{d}\tau \tag{31}$$

The derivation is followed by introducing a Green's function for a moving medium. The starting point is the Green's function given by Blokhintsev [10] for sound radiation in the axial inflow problem, a steady uniform flow, with a flow of Mach number $M_\infty$ in the positive $x_1$ direction,

$$\begin{aligned} G(\vec{x}, t; \vec{y}, \tau) &= \frac{\delta(\tau - t + R/c_0)}{4\pi R'} \\ R &= \frac{-M_\infty (x_1 - y_1) + R'}{\beta^2}, \quad \beta^2 = 1 - M_\infty^2 \\ R' &= \sqrt{(x_1 - y_1)^2 + \beta^2 ((x_2 - y_2)^2 + (x_3 - y_3)^2)} \end{aligned} \tag{32}$$

In this study, this Green's function is easily extended to the case of a flow of arbitrary direction $\vec{M}_\infty$, in the same fashion as for the procedure used by Carley and Fitzpatrick [11],

$$G(\vec{x}, t; \vec{y}, \tau) = \frac{\delta(\tau - t + R/c_0)}{4\pi R^*} \tag{33}$$

The quantity

$$R^* = \frac{1}{\gamma} \sqrt{|\vec{x} - \vec{y}|^2 + \gamma^2 (\vec{M}_\infty \cdot (\vec{x} - \vec{y}))^2} = \frac{1}{\gamma} \sqrt{r^2 + \gamma^2 (\vec{M}_\infty \cdot \vec{r})^2} \tag{34}$$

is the amplitude radius because it fills the role of the 1/distance amplitude decay in (33). The quantity

$$R = \gamma^2 (R^* - \vec{M}_\infty \cdot \vec{r}) \tag{35}$$

is called the phase radius. In the equations above, the distance between the observer and the source position is defined as $\vec{r} = \vec{x} - \vec{y}$ with its value $r$ (see Fig. 2) and

$$\gamma^2 = 1/(1-|\vec{M}_\infty|^2) \tag{36}$$

For the case of zero flight Mach number, both radii $R^*$ and $R$ reduce to the ordinary propagation distance $r$ and Eq. (33) reduces to the standard form for noise propagation in a medium at rest, i.e. $G(\vec{x},t;\vec{y},\tau) = \delta(\tau - t + r/c_0)/4\pi r$.

Substituting the Green's function of Eq. (33) into Eq. (31) gives

$$p'(\vec{x},t,\vec{M}_\infty) = \int_{-\infty}^{t}\int_{-\infty}^{\infty} q(\vec{y},\tau)\frac{\delta(\tau - t + R/c_0)}{4\pi R^*}\mathrm{d}^3\vec{y}\,\mathrm{d}\tau \tag{37}$$

Considering $g = \tau - t + R/c_0$ yields

$$4\pi p'(\vec{x},t,\vec{M}_\infty) = \int_{-\infty}^{t}\int_{-\infty}^{\infty} q(\vec{y},\tau)\frac{\delta(g)}{R^*}\mathrm{d}^3\vec{y}\,\mathrm{d}\tau \tag{38}$$

Let $q(\vec{y},\tau)$ denote the sum of three source terms in the right-hand side of Eq. (24)

$$q(\vec{y},t) = \frac{\partial^2}{\partial x_i \partial x_j}\left[T_{ij}H(f)\right] - \frac{\partial}{\partial x_i}\left[L_i\delta(f)\right] + \frac{\partial}{\partial t}\left[Q\delta(f)\right] \tag{39}$$

Using Eq. (37) results in the formal solution of the differential equation

$$H(f)p'(\vec{x},t,\vec{M}_\infty) = H(f)p'_Q(\vec{x},t,\vec{M}_\infty) + H(f)p'_L(\vec{x},t,\vec{M}_\infty) + H(f)p'_T(\vec{x},t,\vec{M}_\infty) \tag{40}$$

with

$$\begin{aligned}
H(f)p'_Q(\vec{x},t,\vec{M}_\infty) &= \frac{\partial^2}{\partial x_i \partial x_j}\int_{-\infty}^{t}\int_{-\infty}^{\infty}\frac{T_{ij}(\vec{y},\tau)H(f)}{4\pi R^*}\delta(g)d^3\vec{y}\,\mathrm{d}\tau\\
H(f)p'_L(\vec{x},t,\vec{M}_\infty) &= -\frac{\partial}{\partial x_i}\int_{-\infty}^{t}\int_{-\infty}^{\infty}\frac{L_i(\vec{y},\tau)\delta(f)}{4\pi R^*}\delta(g)\mathrm{d}^3\vec{y}\,\mathrm{d}\tau\\
H(f)p'_T(\vec{x},t,\vec{M}_\infty) &= \frac{D}{Dt}\int_{-\infty}^{t}\int_{-\infty}^{\infty}\frac{Q(\vec{y},\tau)\delta(f)}{4\pi R^*}\delta(g)\mathrm{d}^3\vec{y}\,\mathrm{d}\tau
\end{aligned} \tag{41}$$

In this procedure, since $\vec{y}$ and $\vec{x}$ are independent variables, $\partial/\partial x_i$ was taken outside the integral. One can define the surface $S$ in a reference frame so called $\eta$-frame fixed to the body. The motion of points on the surface is fully described in terms of the $\eta$-frame velocity. This data surface is assumed to be a non-deformable surface, without contraction or expansion. Therefore, Eq. (41) is simplified as follows:

$$\begin{aligned}
4\pi p'_Q(\vec{x},t,\vec{M}_\infty) &= \frac{\partial^2}{\partial x_i \partial x_j}\int_{-\infty}^{t}\int_{f>0} T_{ij}(\vec{y}(\vec{\eta},\tau),\tau)\frac{\delta(g)}{R^*}\mathrm{d}V\,\mathrm{d}\tau\\
4\pi p'_L(\vec{x},t,\vec{M}_\infty) &= -\frac{\partial}{\partial x_i}\int_{-\infty}^{t}\int_{S} L_i(\vec{y}(\vec{\eta},\tau),\tau)\frac{\delta(g)}{R^*}\mathrm{d}S\,\mathrm{d}\tau\\
4\pi p'_T(\vec{x},t,\vec{M}_\infty) &= \frac{D}{Dt}\int_{-\infty}^{t}\int_{S} Q(\vec{y}(\vec{\eta},\tau),\tau)\frac{\delta(g)}{R^*}\mathrm{d}S\,\mathrm{d}\tau
\end{aligned} \tag{42}$$

In the following, we concentrate on the loading (2nd term) and thickness (3rd term) contributions, which are dominant in the tone noise of turbo-machines and efficient in case a permeable surface is used,

$$\begin{aligned}
4\pi p'_L(\vec{x},t,\vec{M}_\infty) &= -\frac{\partial}{\partial x_i}\int_{-\infty}^{t}\int_{S} L_i(\vec{y}(\vec{\eta},\tau),\tau)\frac{\delta(g)}{R^*}\mathrm{d}S\,\mathrm{d}\tau\\
4\pi p'_T(\vec{x},t,\vec{M}_\infty) &= \frac{D}{Dt}\int_{-\infty}^{t}\int_{S} Q(\vec{y}(\vec{\eta},\tau),\tau)\frac{\delta(g)}{R^*}\mathrm{d}S\,\mathrm{d}\tau
\end{aligned} \tag{43}$$

## 4. Formulation 1 for a moving medium

The gradient operator in the loading term can be converted to time derivative. This conversion is done based on an identity relating the space and time derivatives of the Green's function of the wave equation. The term $\delta(g)/R^*$ is a function of the source and the observer time and position i.e. $\tau$, $t$ and $\vec{\eta}$,

$$\begin{aligned}
\frac{\partial}{\partial x_i}\left(\frac{\delta(g)}{R^*}\right) &= \frac{\partial}{\partial x_i}\left(\frac{\delta(\tau - t + R/c_0)}{R^*}\right) = \frac{1}{c_0}\frac{\partial R}{\partial x_i}\frac{\delta'(g)}{R^*} - \frac{\partial R^*}{\partial x_i}\frac{\delta(g)}{R^{*2}}\\
&= \frac{1}{c_0}\frac{\tilde{R}_i}{R^*}\delta'(g) - \frac{\tilde{R}^*_i\delta(g)}{R^{*2}}
\end{aligned} \tag{44}$$

where

$$\tilde{R}^*_i = \frac{\partial R^*}{\partial x_i} = \frac{r_i + \gamma^2 (M_{\infty j} r_j) M_{\infty i}}{\gamma^2 R^*} \tag{45}$$

$$\tilde{R}_i = \frac{\partial R}{\partial x_i} = \gamma^2 (\tilde{R}^*_i - M_{\infty i}) \tag{46}$$

On the other hand, one has

$$\frac{1}{c_0}\frac{\partial}{\partial t}\left(\frac{\tilde{R}_i \delta(g)}{R^*}\right) = -\frac{1}{c_0}\frac{\tilde{R}_i}{R^*}\delta'(g) \tag{47}$$

Therefore,

$$\frac{\partial}{\partial x_i}\left(\frac{\delta(g)}{R^*}\right) = -\frac{1}{c_0}\frac{\partial}{\partial t}\left(\frac{\tilde{R}_i \delta(g)}{R^*}\right) - \frac{\tilde{R}^*_i \delta(g)}{R^{*2}} \tag{48}$$

Substituting (48) to (43) gives the loading noise as follows:

$$4\pi p'_L(\vec{x},t,\vec{M}_\infty) = \frac{1}{c_0}\frac{\partial}{\partial t}\int_{-\infty}^{t}\int_S \frac{L_i(\vec{y}(\vec{\eta},\tau),\tau)\tilde{R}_i\delta(g)}{R^*}\mathrm{d}S\mathrm{d}\tau + \int_{-\infty}^{t}\int_S \frac{L_i(\vec{y}(\vec{\eta},\tau),\tau)\tilde{R}^*_i\delta(g)}{R^{*2}}\mathrm{d}S\mathrm{d}\tau \tag{49}$$

or

$$4\pi p'_L(\vec{x},t,\vec{M}_\infty) = \frac{1}{c_0}\frac{\partial}{\partial t}\int_{-\infty}^{t}\int_S \frac{L_R(\vec{y}(\vec{\eta},\tau),\tau)\delta(g)}{R^*}\mathrm{d}S\mathrm{d}\tau \quad + \int_{-\infty}^{t}\int_S \frac{L_{R^*}(\vec{y}(\vec{\eta},\tau),\tau)\delta(g)}{R^{*2}}\mathrm{d}S\mathrm{d}\tau \tag{50}$$

where $L_R = L_i\tilde{R}_i$ and $L_{R^*} = L_i\tilde{R}^*_i$.

For the thickness noise contribution, one can rewrite (48) as follows:

$$4\pi p'_T(\vec{x},t,\vec{M}_\infty) = \left(\frac{\partial}{\partial t} + c_0 M_{\infty i}\frac{\partial}{\partial x_i}\right)\int_{-\infty}^{t}\int_S Q(\vec{y}(\vec{\eta},\tau),\tau)\frac{\delta(g)}{R^*}\mathrm{d}S\mathrm{d}\tau \tag{51}$$

Applying (48) to (51) yields

$$\begin{aligned} 4\pi p'_T(\vec{x},t,\vec{M}_\infty) = {} & \frac{\partial}{\partial t}\int_{-\infty}^{t}\int_S Q(\vec{y}(\vec{\eta},\tau),\tau)\frac{\delta(g)}{R^*}\mathrm{d}S\mathrm{d}\tau - \frac{\partial}{\partial t}\int_{-\infty}^{t}\int_S Q(\vec{y}(\vec{\eta},\tau),\tau)\frac{M_{\infty_i}\tilde{R}_i\delta(g)}{R^*}\mathrm{d}S\mathrm{d}\tau \\ & - \int_{-\infty}^{t}\int_S Q(\vec{y}(\vec{\eta},\tau),\tau)\frac{c_0 M_{\infty i}\tilde{R}^*_i\delta(g)}{R^{*2}}\mathrm{d}S\mathrm{d}\tau \end{aligned} \tag{52}$$

This can be rewritten in a compact form as

$$4\pi p'_T(\vec{x},t,\vec{M}_\infty) = \frac{\partial}{\partial t}\int_{-\infty}^{t}\int_S (1-M_{\infty R})\frac{Q(\vec{y}(\vec{\eta},\tau),\tau)\delta(g)}{R^*}\mathrm{d}S\mathrm{d}\tau \quad - \int_{-\infty}^{t}\int_S c_0 M_{\infty R^*}\frac{Q(\vec{y}(\vec{\eta},\tau),\tau)\delta(g)}{R^{*2}}\mathrm{d}S\mathrm{d}\tau \tag{53}$$

where $M_{\infty R} = M_{\infty i}\tilde{R}_i$ and $M_{\infty R^*} = M_{\infty i}\tilde{R}^*_i$.

In the loading and the thickness equations, in order to integrate over $d\tau$, the methods of generalized function theory (see Farassat [9]) are used:

$$\int_{-\infty}^{t} h(\tau)\delta(g)\mathrm{d}\tau = \left[\frac{h(\tau)}{|\partial g/\partial\tau|}\right]_{g=0} \tag{54}$$

where the notation $[\cdot]_{g=0}$ denotes evaluation of the term in brackets at the root of $g=0$. If $g$ has more than one root, the term is evaluated at each these roots and the solution is the sum of the evaluated terms at each root. For subsonic, the root of $g$ is called as retarded time, i.e.

$$g = \tau - t + \frac{R}{c_0} = 0 \tag{55}$$

yielding

$$\tau = t - \frac{\gamma^2(R^* - \vec{M}_\infty\cdot\vec{r})}{c_0} \tag{56}$$

The partial differentiation of $g$ with respect to $\tau$ yields

$$\frac{\partial g}{\partial\tau} = 1 + \frac{1}{c_0}\frac{\partial R}{\partial\tau} \tag{57}$$

On the other hand

$$\frac{\partial R}{\partial \tau}=\gamma^2\left(\frac{\partial R^*}{\partial \tau}-M_{\infty i}\frac{\partial r_i}{\partial \tau}\right)=\gamma^2\left(\frac{\partial R^*}{\partial \tau}+c_0M_{\infty_i}M_i\right) \tag{58}$$

and

$$\begin{aligned}\frac{\partial R^*}{\partial \tau}&=\frac{-c_0M_ir_i-c_0\gamma^2(M_{\infty i}r_i)(M_{\infty i}M_i)}{\gamma^2R^*}\\&=-c_0M_i\frac{r_i+\gamma^2(M_{\infty j}r_j)M_{\infty i}}{\gamma^2R^*}\end{aligned} \tag{59}$$

where from (45) it will be

$$\frac{\partial R^*}{\partial \tau}=-c_0M_{R^*},\ M_{R^*}=M_i\tilde{R}^*{}_i \tag{60}$$

Substituting Eq. (60) into Eq. (58) gives

$$\frac{\partial R}{\partial \tau}=\gamma^2(-c_0M_i\tilde{R}^*{}_i+c_0M_{\infty i}M_i)=-c_0M_i\left[\gamma^2(\tilde{R}^*{}_i-M_{\infty i})\right] \tag{61}$$

and from Eq. (46)

$$\frac{\partial R}{\partial \tau}=-c_0M_R,\quad M_R=M_i\tilde{R}_i \tag{62}$$

Therefore, Eq. (57) is rewritten as

$$\frac{\partial g}{\partial \tau}=1-M_R \tag{63}$$

One rewrites Eq. (54) as follows:

$$\int_{-\infty}^{t}h(\tau)\delta(g)d\tau=\left[\frac{h(\tau)}{1-M_R}\right]_e \tag{64}$$

In the above, subscript $e$ indicates that all the values have to be taken at the retarded (emission) time. This relation is applied to the loading and thickness noise expressions (50) and (53), giving

$$\begin{aligned}4\pi p_L'(\vec{x},t,\vec{M}_\infty)&=\frac{1}{c_0}\frac{\partial}{\partial t}\int_S\left[\frac{L_R}{R^*(1-M_R)}\right]_e\mathrm{d}S+\int_S\left[\frac{L_{R^*}}{R^{*2}(1-M_R)}\right]_e\mathrm{d}S\\4\pi p_T'(\vec{x},t,\vec{M}_\infty)&=\frac{\partial}{\partial t}\int_S\left[\frac{(1-M_{\infty R})Q}{R^*(1-M_R)}\right]_e\mathrm{d}S-\int_S\left[\frac{c_0M_{\infty R^*}Q}{R^{*2}(1-M_R)}\right]_e\mathrm{d}S\end{aligned} \tag{65}$$

Eq. (65) explicitly takes into account the convection effect. This formulation is equivalent to the formulation 1 of Farassat if the medium is at rest, $\vec{M}_\infty=0$. It is worth adding that in case the source moves with $\vec{M}$ in a plane and the flow $\vec{M}_\infty$ is perpendicular to that plane, the scalar product of $\vec{M}$ and $\vec{M}_\infty$ is equal to zero and there is no convection effect on the Doppler factor.

The time domain moving medium formulation given by (65), explicitly takes into account the mean flow influence and the aerodynamic and acoustic effects of incidence. This formulation is derived with Doppler factor because it is more easily interpreted and is more helpful in examining the physic of systems. Based on this approach, the source of asymmetry of the sound field can be explained in terms of physics of a moving source.

## 5. Formulation 1A for a moving medium

The next modification consists in moving the time derivative inside the integrals. This can be made based on the retarded time definition given in Eq. (56) and using the following rules:

$$\left.\frac{\partial \tau}{\partial t}\right|_{\vec{x}}=\frac{\partial}{\partial t}\left(t-\frac{R}{c_0}\right)\Big|_{\vec{x}}=1-\frac{1}{c_0}\left.\frac{\partial R}{\partial t}\right|_{\vec{x}} \tag{66}$$

$$\left.\frac{\partial R}{\partial t}\right|_{\vec{x}}=\frac{\partial R}{\partial y_i}\frac{\partial y_i}{\partial \tau}\left.\frac{\partial \tau}{\partial t}\right|_{\vec{x}}=-c_0M_i\tilde{R}_i\left.\frac{\partial \tau}{\partial t}\right|_{\vec{x}}=-c_0M_R\left.\frac{\partial \tau}{\partial t}\right|_{\vec{x}} \tag{67}$$

From (66) and (67) one has

$$\left.\frac{\partial}{\partial t}\right|_{\vec{x}}=\frac{1}{1-M_R}\left.\frac{\partial}{\partial \tau}\right|_{\vec{x}}=\left(\frac{1}{1-M_R}\left.\frac{\partial}{\partial \tau}\right|_{\vec{x}}\right)_e \tag{68}$$

where the term $(1-M_R)_e$ accounts for a dilatation or contraction of the observer time scale with respect to the source time scale, depending on whether the source moves far away from or towards the observer, respectively. As already mentioned,

this effect is known as Doppler effect. One can also have the relations (given at the retarded time),

$$\frac{\partial \tilde{R}^*_i}{\partial \tau} = \frac{-c_0 M_i + c_0\gamma^2(M_{R^*}\tilde{R}^*_i - M_{\infty M}M_{\infty i})}{\gamma^2 R^*}\frac{\partial \tilde{R}_i}{\partial \tau} = \gamma^2\frac{\partial \tilde{R}^*_i}{\partial \tau} \tag{69}$$

$$\frac{\partial \tilde{R}^*_i}{\partial x_j} = \frac{\partial r_i/\partial x_j + \gamma^2(M_{\infty i}M_{\infty j} - \tilde{R}^*_i\tilde{R}^*_j)}{\gamma^2 R^*}\frac{\partial \tilde{R}_i}{\partial x_j} = \gamma^2\frac{\partial \tilde{R}^*_i}{\partial x_j} \tag{70}$$

and

$$\frac{\partial M_R}{\partial \tau} = \frac{R^*\dot{M}_R + c_0(\gamma^2 M^2_{R^*} - M^2)}{R^*} - \frac{c_0\gamma^2 M^2_{\infty M}}{R^*} \tag{71}$$

where $M_{\infty M} = M_{\infty i}M_i$ and $\dot{M}_R = \dot{M}_i\tilde{R}_i$. The dot over the term denotes the derivative with respect to the source time $\tau$. The following explicit derivations are valid for subsonic flow cases.

### 5.1. Thickness noise

Taking the time derivate inside the integral of the thickness source and using (68) yields

$$4\pi p'_T(\vec{x},t,\vec{M}_\infty) = \int_S \frac{1}{1-M_R}\frac{\partial}{\partial \tau}\left[\frac{(1-M_{\infty R})Q}{R^*(1-M_R)}\right]_e \mathrm{d}S - \int_S \left[\frac{c_0 M_{\infty R}Q}{R^{*2}(1-M_R)}\right]_e \mathrm{d}S \tag{72}$$

It can be rewritten as

$$\begin{aligned} 4\pi p'_T(\vec{x},t,\vec{M}_\infty) = {} & \int_S \left[\frac{(1-M_{\infty R})\dot{Q}}{R^*(1-M_R)^2}\right]_e \mathrm{d}S - \int_S \left[Q\frac{-M_{\infty i}\partial \tilde{R}_i/\partial \tau}{R^*(1-M_R)^2}\right]_e \mathrm{d}S \\ & + \int_S \left[Q\frac{(1-M_{\infty R})}{R^*(1-M_R)}\right]_e \frac{\partial}{\partial \tau}\left[\frac{1}{(1-M_R)}\right]_e \mathrm{d}S - \int_S \left[\frac{c_0 M_{\infty R}Q}{R^{*2}(1-M_R)}\right]_e \mathrm{d}S \end{aligned} \tag{73}$$

where $\dot{Q} = \partial Q/\partial \tau$. One obtains

$$\begin{aligned} \frac{\partial}{\partial \tau}\left[\frac{1}{R^*(1-M_R)}\right] &= \left[\frac{-1}{R^{*2}(1-M_R)}\frac{\partial R^*}{\partial \tau} + \frac{1}{R^*(1-M_R)^2}\frac{\partial M_R}{\partial \tau}\right] \\ &= \left[\frac{R^*\dot{M}_R + c_0(M_{R^*} - M^2)}{R^{*2}(1-M_R)^2}\right] - \left[\frac{c_0 M_{R^*}(M_R - \gamma^2 M_{R^*}) + c_0\gamma^2 M^2_{\infty M}}{R^{*2}(1-M_R)^2}\right] \end{aligned} \tag{74}$$

and uses Eq. (60) to have

$$\begin{aligned} 4\pi p'_T(\vec{x},t,\vec{M}_\infty) = {} & \int_S \left[\frac{(1-M_{\infty R})\dot{Q}}{R^*(1-M_R)^2}\right]_e \mathrm{d}S + \int_S \left[(1-M_{\infty R})Q\frac{R^*\dot{M}_R + c_0(M_{R^*} - M^2)}{R^{*2}(1-M_R)^3}\right]_e \mathrm{d}S \\ & - \int_S \left[(1-M_{\infty R})Q\frac{c_0 M_{R^*}M_R + c_0\gamma^2(M^2_{\infty M} - M^2_{R^*})}{R^{*2}(1-M_R)^3}\right]_e \mathrm{d}S \\ & - \int_S \left[Q\frac{c_0\gamma^2(M_{\infty R^*}M_{R^*} - M_{\infty M})}{R^{*2}(1-M_R)^2}\right]_e \mathrm{d}S - \int_S \left[Q\frac{c_0 M_{\infty R^*}}{R^{*2}(1-M_R)}\right]_e \mathrm{d}S \end{aligned} \tag{75}$$

### 5.2. Loading noise

Applying relation (68) to the dipole term of Eq. (65) results in the following expression:

$$4\pi p'_L(\vec{x},t,\vec{M}_\infty) = \frac{1}{c_0}\int_S \left[\frac{1}{1-M_R}\right]_e \frac{\partial}{\partial \tau}\left[\frac{L_R}{R^*(1-M_R)}\right]_e \mathrm{d}S + \int_S \left[\frac{L_{R^*}}{R^{*2}(1-M_R)}\right]_e \mathrm{d}S \tag{76}$$

On the right-hand side, taking the time derivative gives

$$\frac{\partial}{\partial \tau}\left[\frac{L_R}{R^*(1-M_R)}\right] = \frac{\dot{L}_R}{R^*(1-M_R)} + \frac{L_i\partial \tilde{R}_i/\partial \tau}{R^*(1-M_R)} + L_R\frac{\partial}{\partial \tau}\left(\frac{1}{1-M_R}\right) \tag{77}$$

where $L_R = L_i\tilde{R}_i$, $\dot{L}_R = \dot{L}_i\tilde{R}_i$ and $\dot{L}_i = \partial L_i/\partial \tau$. Having the relation (69), sum of the second terms on the right-hand side of Eqs. (76) and (77) becomes,

$$\frac{L_{R^*}}{R^{*2}(1-M_R)} + \frac{L_i\partial \tilde{R}_i/\partial \tau}{R^*(1-M_R)^2} = \frac{L_{R^*} - L_M - L_{R^*}(M_R - \gamma^2 M_{R^*}) - \gamma^2 M_{\infty M}M_{\infty L}}{R^{*2}(1-M_R)^2} \tag{78}$$

Substituting (74) to (77) and rearranging Eqs. (76) to (78) yield,

$$4\pi p'_L(\vec{x},t,\vec{M}_\infty)=\frac{1}{c_0}\int_S\left[\frac{\dot{L}_R}{R^*(1-M_R)^2}\right]_e \mathrm{d}S+\int_S\left[\frac{L_{R^*}-L_M}{R^{*2}(1-M_R)^2}\right]_e \mathrm{d}S+\frac{1}{c_0}\int_S\left[L_R\frac{R^*\dot{M}_R+c_0(M_{R^*}-M^2)}{R^{*2}(1-M_R)^3}\right]_e \mathrm{d}S$$
$$-\int_S\left[L_R\frac{M_{R^*}M_R+\gamma^2(M^2_{\infty M}-M^2_{R^*})}{R^{*2}(1-M_R)^3}\right]_e \mathrm{d}S-\int_S\left[\frac{L_{R^*}M_R+\gamma^2(M_{\infty M}M_{\infty L}-L_{R^*}M_{R^*})}{R^{*2}(1-M_R)^2}\right]_e \mathrm{d}S \tag{79}$$

Finally, the overall acoustic pressure, which consists in the thickness contribution obtained with Eq. (75) and the dipole contribution obtained with Eq. (79), is given by

$$p'(\vec{x},t,\vec{M}_\infty)=\underbrace{p'_L(\vec{x},t,\vec{M}_\infty)}_{loading}+\underbrace{p'_T(\vec{x},t,\vec{M}_\infty)}_{thickness} \tag{80}$$

with

$$4\pi p'_L(\vec{x},t,\vec{M}_\infty)=\frac{1}{c_0}\int_S\left[\frac{\dot{L}_R}{R^*(1-M_R)^2}\right]_e \mathrm{d}S+\int_S\left[\frac{L_{R^*}-L_M}{R^{*2}(1-M_R)^2}\right]_e \mathrm{d}S+\frac{1}{c_0}\int_S\left[L_R\frac{R^*\dot{M}_R+c_0(M_{R^*}-M^2)}{R^{*2}(1-M_R)^3}\right]_e \mathrm{d}S$$
$$-\int_S\left[L_R\frac{M_{R^*}M_R+\gamma^2(M^2_{\infty M}-M^2_{R^*})}{R^{*2}(1-M_R)^3}\right]_e \mathrm{d}S-\int_S\left[\frac{L_{R^*}M_R+\gamma^2(M_{\infty M}M_{\infty L}-L_{R^*}M_{R^*})}{R^{*2}(1-M_R)^2}\right]_e \mathrm{d}S$$
$$4\pi p'_T(\vec{x},t,\vec{M}_\infty)=\int_S\left[\frac{(1-M_{\infty R})\dot{Q}}{R^*(1-M_R)^2}\right]_e \mathrm{d}S+\int_S\left[(1-M_{\infty R})Q\frac{R^*\dot{M}_R+c_0(M_{R^*}-M^2)}{R^{*2}(1-M_R)^3}\right]_e \mathrm{d}S$$
$$-\int_S\left[(1-M_{\infty R})Q\frac{c_0M_{R^*}M_R+c_0\gamma^2(M^2_{\infty M}-M^2_{R^*})}{R^{*2}(1-M_R)^3}\right]_e \mathrm{d}S-\int_S\left[\frac{c_0\gamma^2(M_{\infty R^*}M_{R^*}-M_{\infty M})Q}{R^{*2}(1-M_R)^2}\right]_e \mathrm{d}S-\int_S\left[\frac{c_0M_{\infty R^*}Q}{R^{*2}(1-M_R)}\right]_e \mathrm{d}S \tag{81}$$

where

$$L_i=\rho\, u_i[u_n-(v_n-U_{\infty n})]+P_{ij}\hat{n}_j$$
$$Q=\rho[u_n-(v_n-U_{\infty n})]+\rho_0(v_n-U_{\infty n}) \tag{82}$$

The sources defined in Eq. (82) omit the quadrupole term, so all significant nonlinear sources is contained within a permeable surface. For an impermeable surface, such as the actual blade surface, the sources reduce to

$$L_i=P_{ij}\hat{n}_j$$
$$Q=\rho_0(v_n-U_{\infty n}) \tag{83}$$

The formulation given by (81) is an extension of formulation 1A of Farassat to a moving medium case. This formulation is numerically more efficient since the numerical time derivative has been eliminated. It is valid for arbitrary body motion and geometry in a steady uniform flow with arbitrary orientations. The terms inside the summations are calculated for the retarded time. The dot over a symbol implies differentiation of this magnitude in respect to the emission time. The summations with $1/R^*$ and $1/R^{*2}$ dependence are the far field and near field terms, respectively. As can be seen, the presence of the mean flow affects the near field more than the far field for both the thickness noise and the loading noise.

The formulation shows explicitly the effect of incidence on the Doppler amplification of the radiated noise. It allows the convective effect on propeller noise to be decoupled from the rotational and unsteady loading effects. The remarkable feature of the formulation is that it provides a way of examining the physics of the problem and enables us to process asymmetric inflow effects. The source of asymmetry of the sound field can be explained in terms of the physics of a moving source rather than in terms of spinning modes. It is worth adding that Hanson and Paryzch [6] and Hanson [5] have used the same approach to develop exact frequency domain formulations, which include the convective effect at an angle of attack.

## 6. Stationary permeable data surfaces

The simple case of a stationary data surface is commonly used in the hybrid CFD/acoustic analogy approach. In this case, $v_i=0$ and the formulations of (65) become

$$4\pi p'_T(\vec{x},t,\vec{M}_\infty)=\frac{\partial}{\partial t}\int_S\left[(1-M_{\infty R})\frac{Q}{R^*}\right]_e \mathrm{d}S-\int_S\left[c_0M_{\infty R^*}\frac{Q}{R^{*2}}\right]_e \mathrm{d}S$$
$$4\pi p'_L(\vec{x},t,\vec{M}_\infty)=\frac{1}{c_0}\frac{\partial}{\partial t}\int_S\left[\frac{L_R}{R^*}\right]_e \mathrm{d}S+\int_S\left[\frac{L_{R^*}}{R^{*2}}\right]_e \mathrm{d}S \tag{84}$$

Similarly, the formulations of (81) reduce to

$$4\pi p'_T(\vec{x},t,\vec{M}_\infty)=\int_S\left[\frac{(1-M_{\infty R})\dot{Q}}{R^*}\right]_e \mathrm{d}S-\int_S\left[Q\frac{c_0M_{\infty R^*}}{R^{*2}}\right]_e \mathrm{d}S$$

$$4\pi p'_L(\vec{x},t,\vec{M}_\infty)=\frac{1}{c_0}\int_S\left[\frac{\dot{L}_R}{R^*}\right]_e \mathrm{d}S+\int_S\left[\frac{L_{R^*}}{R^{*2}}\right]_e \mathrm{d}S \tag{85}$$

In this case, the emission distance between the observer and the source is constant, and the radius $R$ does not depend on the retarded time. Therefore, the retarded time is obtained with an explicit solution, where no iterative method is needed. This reduces the computational time.

## 7. Numerical implementation and verification test cases

The acoustic computations are carried out in an acoustic module based on the derived formulation. The implementation is specified for the problem of a propeller at incidence. The acoustic module uses the flow data, which is necessary for the acoustics, as inputs. The module computes the acoustic pressure signature, directivity and overall sound pressure. At the end of the computation, the far-field acoustic signal is analyzed in the frequency domain. The retarded time method is chosen to treat the relationship between the source and observation time. In order to perform time derivations required in integrals, a second-order accurate method is used.

The sound levels can be very sensitive to the accuracy of the computed retarded time, the position of the moving sources and mean flow effects, especially for highly unsteady loads. Therefore, severe validation and verification tests are required. The verification can be ideally carried out with the aid of analytical solutions of the governing equations, because the numerical errors are easy to be calculated through the comparison between the numerical and analytical solutions. In the present context, five verification test cases are chosen. The test cases are as follows: a wind-tunnel case with a monopole source, a wind-tunnel case with a dipole source, a rotating point force in crossflow, a model of a helicopter blade at incidence and a very interesting consistency test, known as the Isom thickness noise [12,13] for propellers at incidence.

### 7.1. TC1: wind-tunnel case with a monopole source

The first validation problem is a wind-tunnel case, where the source is stationary, but the flow is moving with a constant velocity. This test case is for the validation of the developed formulation when applied to a permeable data surface. Consider a single-frequency monopole source located at the origin in a uniform flow with an arbitrary orientation. Dowling and Ffowcs Williams [14] have obtained the complex potential for the monopole in a uniform flow in the $x_1$ direction as follows:

$$\varphi(x_1,t)=A\frac{1}{4\pi R'}\exp\left[i\omega\left(t-\frac{R'-M_\infty x_1}{c_0}\right)\right] \tag{86}$$

If the source is positioned at origin one has

$$R'=\sqrt{x_1^2+\beta^2(x_2^2+x_3^2)},\quad \beta^2=1-M_\infty^2 \tag{87}$$

In this work, the complex potential for the monopole is extended and adapted to an equivalent flow in which the source is fixed at the origin and the uniform flow has an arbitrary orientation. The extended form of the velocity potential is defined as follows:

$$\varphi(\vec{x},t)=A\frac{1}{4\pi R^*}\exp\left[i\omega\left(t-\frac{R}{c_0}\right)\right] \tag{88}$$

where the radiuses $R^*$ and $R$ are obtained from Eqs.(34) and (35). The acoustic particle velocity can be obtained by the gradient of the velocity potential

$$u_i(\vec{x},t)=\frac{\partial\varphi(\vec{x},t)}{\partial x_i} \tag{89}$$

where the spatial derivatives of $R^*$ and $R$ can be computed using Eqs. (45) and (46), respectively. The acoustic pressure, for the case with a mean flow of $\vec{M}_\infty$, is described by the unsteady Bernoulli equation

$$p'(\vec{x},t)=-\rho_0\left(\frac{\partial\varphi(\vec{x},t)}{\partial t}+c_0M_{\infty i}\frac{\partial\varphi(\vec{x},t)}{\partial x_i}\right)=-\rho_0\left(i\omega+c_0M_{\infty i}\frac{\partial}{\partial x_i}\right)\varphi(\vec{x},t) \tag{90}$$

and the induced density is given by $\rho'(\vec{x},t)=p'(\vec{x},t)/c_0^2$.

Here, the velocity potential amplitude is $A=1\ \mathrm{m}^2/\mathrm{s}$. The angular frequency $\omega$ of the source is $(34\,\pi)$ rad/s. The ambient speed of sound $c_0$ is chosen as 340.75 m/s. The free stream flow density is assumed to be $1.234\ \mathrm{kg/m}^3$. A spherical penetrable surface is used as the data surface for this test case. The spherical permeable surface used has a radius of 1 m. The polar azimuthal angle $\theta$ and polar angle $\varphi$ are discretized into 121 and 91 grids, respectively. The grids are well-distributed on the spherical surface. The temporal resolution is fine enough, where $\Delta t/T$ is smaller than 0.02. The radiated sound pressure is recorded at a distance of 20 m from the source for different mean flow orientations.

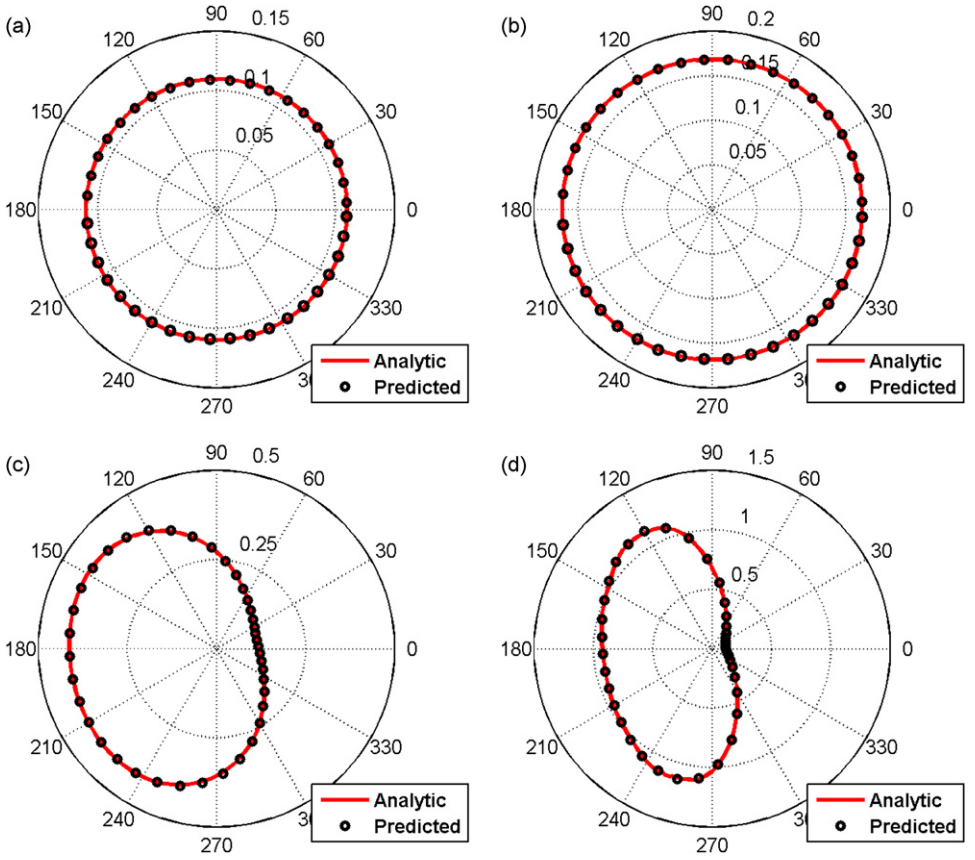


**Fig. 3.** Comparison of the root mean square of the predicted monopole acoustic pressure with that of the analytical solution is shown for different inflow Mach numbers. $r=20$ m: (a)$\vec{M}_\infty=(0,0,0)$, (b) $\vec{M}_\infty=(0,0,0.5)$, (c) $\vec{M}_\infty=(0.5,0.1,0.5)$ and (d) $\vec{M}_\infty=(0.7,0.1,0.5)$.

Fig. 3 shows a comparison of the root mean square of the monopole acoustic pressure at 20 m for the exact solution and for the prediction. The predicted result agrees very well with the exact solution for different mean flow Mach numbers. This result demonstrates that the permeable surface prediction by the developed formulation is correct.

It is worth adding that if the source is moving in a plane (with $\vec{M}$) and the flow $\vec{M}_\infty$ is perpendicular to that plane, the scalar product of $\vec{M}$ and $\vec{M}_\infty$ is equal to zero and there is no convection effect on the Doppler factor. We have shown this case in Fig. 3(b), where the source is in the $x_1$,$x_2$-plane and the flow $\vec{M}_\infty=(0,0,0.5)$ is perpendicular to this plane. It can also be seen that increasing Mach number in the $x_1$ direction increases the convective effect on the noise propagation, making the level of acoustic pressure at a point in upstream greater than the corresponding point in downstream. The same conclusion can be made for $x_2$ direction.

Fig. 4 shows a comparison of the acoustic pressure for the exact solution, the predictions with the obtained formulation and the moving observer method. It can be seen that the prediction can match extremely well the exact solution. This result confirms that the derived formulation can be used to accurately compute the acoustic pressure for a source case in a moving medium.

### 7.2. TC2: wind-tunnel case with a dipole source

The second validation test case is a wind tunnel case with a stationary dipole point source located in a moving medium with arbitrary orientation. We consider that the dipole axis is aligned with the $x_2$-axis. Using the extended form of the velocity potential of the aforementioned monopole case, one can obtain the velocity potential for such case as follows:

$$\varphi(\mathrm{x},t)=\left(\frac{\tilde{R}^*_2}{R^*}+\frac{\omega\tilde{R}_2}{c_0}\right)\left\{A\frac{1}{4\pi R^*}\exp\left[i\omega\left(t-\frac{R}{c_0}\right)\right]\right\} \tag{91}$$

where $\tilde{R}^*_2$ and $\tilde{R}_2$ are obtained from Eqs. (45) and (46). The procedure of making the acoustic pressure predictions is similar to that used for the stationary point monopole. For noise calculation, one might need the following expressions:

$$\frac{\partial\tilde{R}^*_2}{\partial x_1}=\frac{\gamma^2(M_{\infty 2}M_{\infty 1}-\tilde{R}^*_2\tilde{R}^*_1)}{\gamma^2 R^*}$$

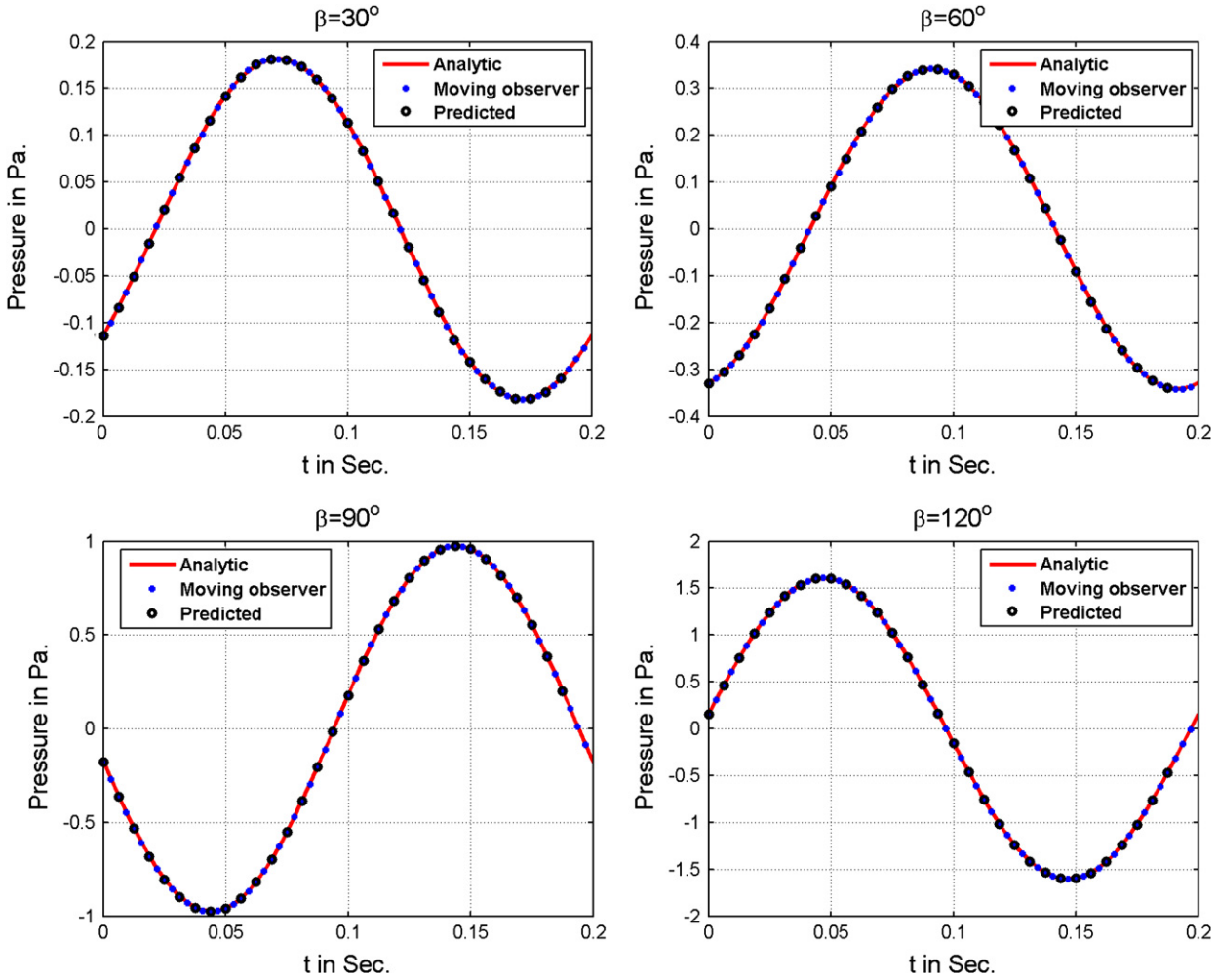


**Fig. 4.** The calculated monopole acoustic pressure time history compared with that of the moving observer method and analytical solution is shown for different observer positions. $r=20$ m: $\vec{M}_\infty=(0.7,0.1,0.5)$.

$$\frac{\partial \tilde{R}_2^*}{\partial x_2}=\frac{1+\gamma^2(M_{\infty 2}M_{\infty 2}-\tilde{R}_2^{*2})}{\gamma^2 R^*}$$

$$\frac{\partial \tilde{R}_2^*}{\partial x_3}=\frac{\gamma^2(M_{\infty 2}M_{\infty 3}-\tilde{R}_2^*\tilde{R}_3^*)}{\gamma^2 R^*} \tag{92}$$

and

$$\frac{\partial \tilde{R}_2}{\partial x_i}=\gamma^2\frac{\partial \tilde{R}_2^*}{\partial x_i} \tag{93}$$

A spherical permeable surface enclosing the point source is created and flow passes by the surface with Mach number $\vec{M}_\infty$. The pressure, density and velocity evaluated on the surface are used for the prediction of the acoustic pressure. Again, $A=1$ is used in this problem. The source frequency is $\omega=10\pi$ rad/s. The ambient speed of sound $c_0$ is set to be 340.75 m/s. The free stream flow density is equal to 1.234 kg/m$^3$. The radiated sound pressure is recorded at a distance of 100 m from the source. Different mean flow orientations are used.

Fig. 5 shows a comparison of the root mean square of the dipole acoustic pressure with that of the exact solution for different observer positions. Different Mach number cases are used for this comparison. It can be seen that the prediction can match extremely well, such that the exact solution so that each line can barely be distinguished on this graph. The agreement between the present prediction and the exact solution is excellent for different inflow configurations.

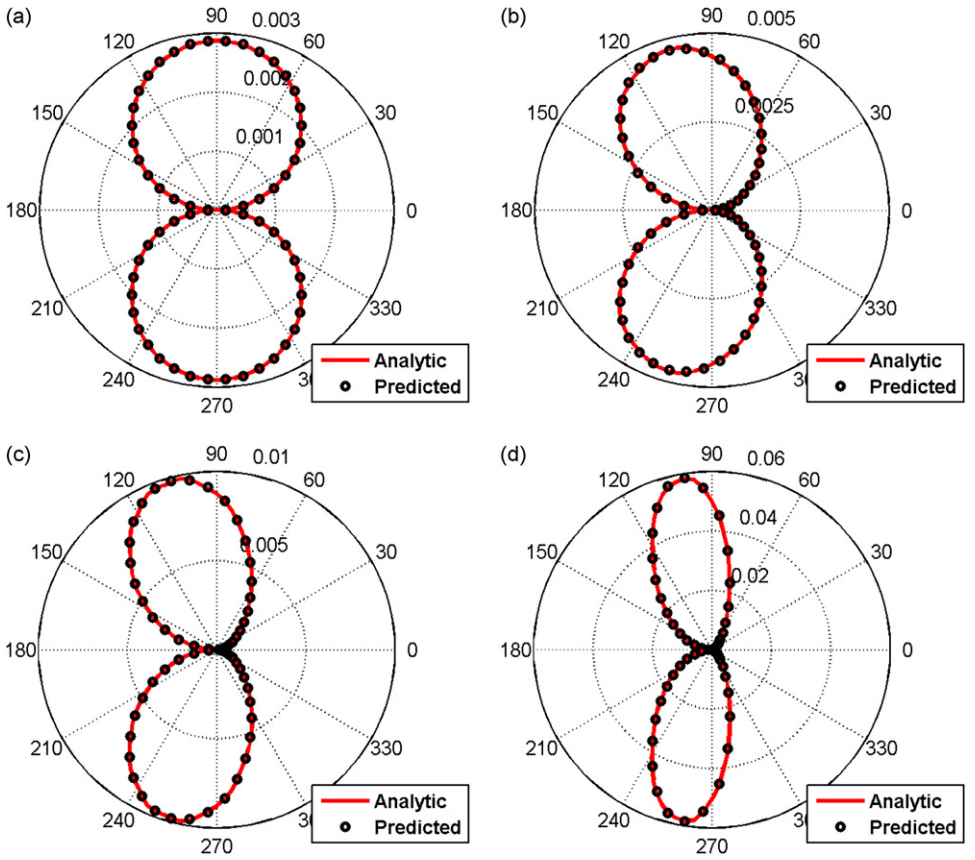


**Fig. 5.** Comparison of the root mean square of the predicted dipole acoustic pressure with that of the analytical solution is shown for different inflow Mach numbers. $r=100$ m: (a) $\vec{M}_\infty=(0,0,0.4)$, (b) $\vec{M}_\infty=(0.4,0,0.4)$, (c) $\vec{M}_\infty=(0.6,0,0.4)$ and (d) $\vec{M}_\infty=(0.8,0,0.4)$.

### 7.3. TC3: sound from a rotating source in crossflow

The third test case is a model for a simple point source case for a compact moving dipole described by Rienstra and Hirschberg [15]. An application of this case is a model for (subsonic) propeller noise, due to Farassat and Succi [3]. It consists of a subsonic dipole $f_0$, rotating in the $x_2$-, $x_3$-plane along a circle of radius $a$ with frequency $\omega$ and translating with a constant velocity of $U$ along the axis of rotation $x_1$.

In order to define a more representative test case of rotating and translating point source, a variant of this test case is defined by considering an angle of attack in its motion. The test case can be presented as a rotating point dipole source in moving medium with inflow angle of $\alpha$. As shown in Fig. 6, the inflow velocity vector can be aligned at an arbitrary angle to the propeller axis, i.e.

$$\vec{U}_\infty=(-U\cos\alpha,0,-U\sin\alpha) \tag{94}$$

The rotating point force portrays a very simple propeller model. The propeller is assumed to be concentrated in one point by a point force equal to the blade thrust force (the pressure jump across the blade integrated over the blade), in a direction perpendicular to the blade. This model is a plausible approximation for the lowest harmonics.

In order to check the feasibility of the moving medium method for rotor-noise prediction, the blade surface should be defined. The blade surface will practically coincide with a screw plane described by the effective velocity field (point source velocity relative to the fluid) given by

$$\vec{V}=U\cos\alpha\hat{i}+a\omega\sin\omega t\hat{j}+(a\omega\cos\omega t+U\sin\alpha)\hat{k} \tag{95}$$

The compact dipole source is described as this screw plane with a pressure jump uniformly distributed on its surface:

$$\vec{f}=f_0\hat{n} \tag{96}$$

where the surface unit vector $\hat{n}$ is defined as follows:

$$\hat{n}=\frac{1}{\sqrt{U^2+(a\omega)^2}}\,(A,U\cos\alpha\sin\varphi,-U\cos\alpha\cos\varphi) \tag{97}$$

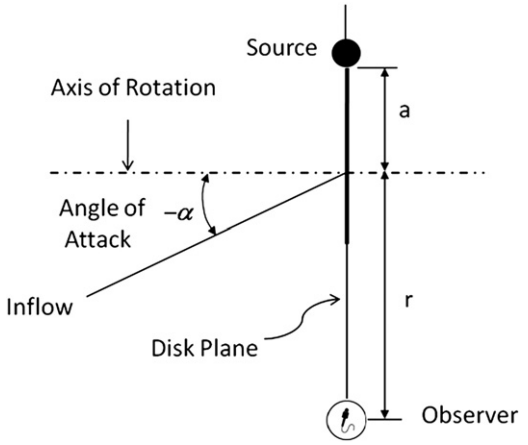


**Fig. 6.** Schematic of rotating point source.

with

$$\sin\varphi = a\omega\sin\omega t/A$$
$$\cos\varphi = (a\omega\cos\omega t + U\sin\alpha)/A$$
$$A = \sqrt{U^2\sin^2\alpha + (a\omega)^2 + 2a\omega U\sin\alpha\cos\omega t} \tag{98}$$

The center of the plane is assumed to be in the position of the compact source. The rotational velocity is kept constant at the value $\omega = (34\pi)\,\mathrm{rad/s}$. The observer is assumed to be stationary in the moving medium with flow over. The following parameters are used in the computations: $f_0 = 700N$, $c_0 = 316$ m/s, $\rho_0 = 1.2$ kg/m$^3$, $U = 145$ m/s and $a = 1.28m$.

The noise calculation is carried out for this model with 128 time points per acoustic period for an observer positioned at $\vec{x} = (0,-2.5,0)m$. Fig. 7 shows the calculated dipole pressure for different angles of attack. For comparison, the results from the solution described in [15] are plotted in this figure. There is a very good agreement between the results for different angles of attack. Comparisons verify the accuracy of the method for prediction of noise radiated from rotating source at incidence.

### 7.4. TC4: model of helicopter blade with angle of attack

The fourth test case, which is a conventional helicopter rotor, considers a reference solution obtained by Brentner [16] as part of the NASA WOPWOP code. The helicopter rotor is a 1/4-scale UH-1 rotor model and consists of two NACA0012 airfoil section blades at an angular velocity of 1296 rev/min. The blades are 1.829 m in diameter with a constant chord of 0.1334 m. The cutout blade radius is 0.155 m. The rotor blade is twisted along its length, with a linear twist with angle of $-10^\circ$. The flapping angle $\beta$, the feathering angle $\theta$ and the led-lag angle $\varsigma$ are presented in the most general case of forward flight by Fourier series that includes a constant term and the first and second harmonics. For the present test case,

$$\beta = 2.72 - 1.5\cos\theta_b + 1.18\sin\theta_b$$
$$\theta = 13.82 + 2.2\cos\theta_b - 1.47\sin\theta_b$$
$$\varsigma = 0 \tag{99}$$

where $\theta_b$ is the azimuthal angle measured from tail of helicopter in counterclockwise direction when looking from above (see Fig. 2). The noise is calculated in a ground fixed frame. Fig. 8 shows the reference frame GF, which is fixed to the ground so that the $GF_3$ axis oriented as the rotor shaft, i.e. rotated at an angle $\alpha$ with respect to the ground. The frame MF is oriented in the same fashion as the previous one but is translated with a velocity $\vec{V}_H$ and with the origin on the rotor shaft.

From the discussion above, it is clear that for any type of helicopter rotor, the degrees of freedom of the rotor's blades comprise at least flapping, feathering and the lead/lagging motion. This means that the motion of a reference frame connected to the main rotor blades with respect to the observer frame must include at least all the above degrees of freedom in addition to rotation and translation with respect to the ground fixed reference frame.

In the moving medium technique, the observer is assumed to be fixed on the ground fixed frame and the translating degree of freedom is replaced by flow motion over the blade. The angle of attack is set to be $\alpha = -8.85^o$. The observer position and the inflow Mach number vector are given in the OF as follows:

$$\vec{x}_{obs} = (3.21,-2.16,-0.3)m \tag{100}$$

and

$$\vec{V}_H = (51.5,0,0)m/s \tag{101}$$

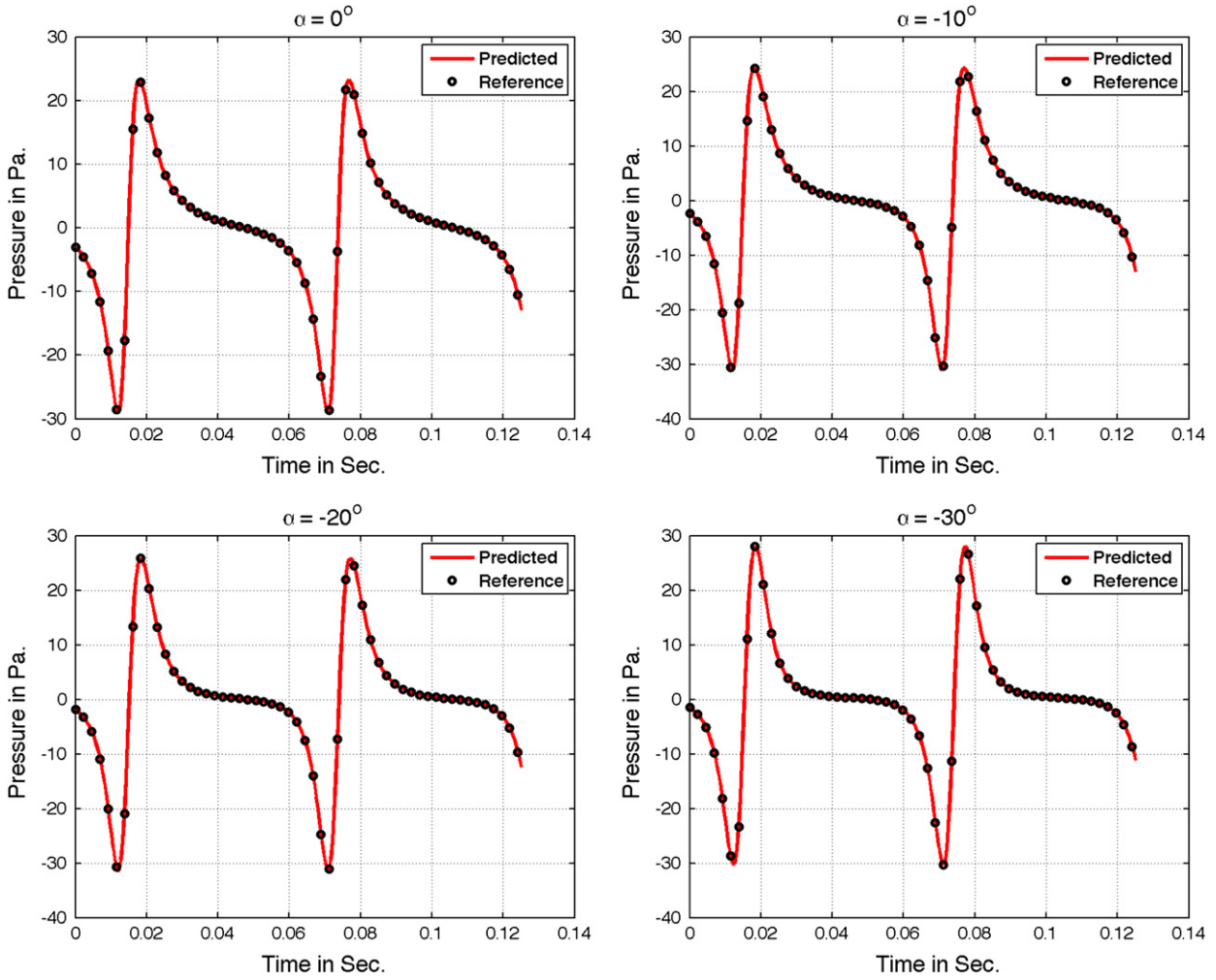


**Fig. 7.** Comparison of the predicted dipole acoustic pressure with that of the analytical solution is shown for different inflow angles. $r = 2.5$ m.

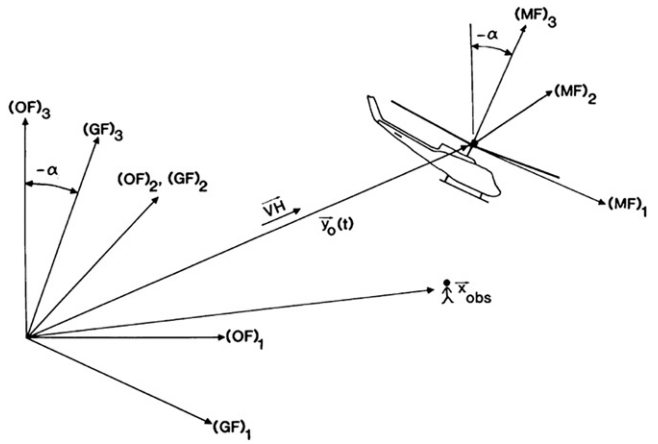


**Fig. 8.** Description of intermediate coordinates for rotating and translating blades.

This is a case in which thickness noise is impulsive and dominates the overall noise. Therefore, the moving medium technique is applied to this test case and the thickness noise is calculated. The noise calculation is performed in the ground fixed frame GF. Using the transformation matrix from OF to GF (see Fig. 8), the observer position and the inflow Mach

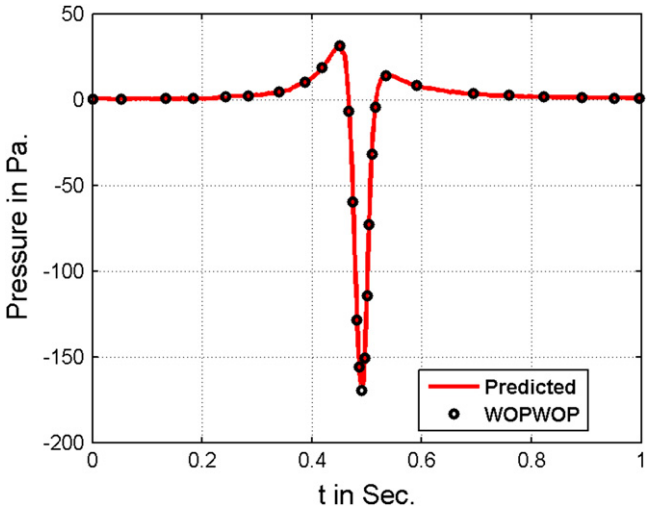


**Fig. 9.** The calculated thickness noise time history compared with that of WOPWOP for the blades (NACA0012) operating at incidence is shown.

number vector $(-\vec{V}_H/c_0)$ are obtained in the GF. The following parameters are used for the noise calculations: $c_0 = 340$ m/s, and $\rho_0 = 1.234$ kg/m$^3$.

The blade surface is discretized into 120 cells around the blade airfoil and 100 divisions along the radial direction for the complete convergence. A non-uniform mesh density is used in both directions. The calculation is performed for 128 time points per blade passage to resolve the pressure time history. The computed thickness noise is plotted in Fig. 9. For comparison, the results from the NASA WOPWOP code is also illustrated in this figure. As can be seen, the result from the moving medium technique and that of the WOPWOP code mach each other quite well. This agreement validates the accuracy of the developed formulations.

### *7.5. TC5: Isom thickness noise for propellers at incidence*

Isom thickness noise property is described in the review paper of Brentner and Farassat [17]. It is demonstrated that if a constant aerodynamic load, $p = \rho_0 c_0^2$ is applied over a moving surface the generated dipole noise should be identical to the monopole thickness noise contribution. Consequently, the calculation of the thickness noise becomes completely independent of the normal velocity $v_n$ over the surface.

This consistency has already been tested for a conventional helicopter blade [18]. It was shown that by including the blade tip source and refining the grid at the inner and outer radii of the blade the calculated Isom noise results match the monopole noise results quite well. It was also indicated that by decreasing the thickness ratio at the extremities of the blade the calculate results agree with the theory.

The previous study dealt with evaluating the Isom thickness noise property for rotating blades in a medium at rest. To the knowledge of the authors, the Isom thickness noise property has never been tested for rotating blades in cross flow. In the present paper, we focus on the evaluation of this test case in presence of a mean flow with an arbitrary orientation. This consistency test for moving medium problems will bring more detailed analysis of the Isom noise behavior of the rotating blades against the mean flow and the angle of incidence.

The numerical strategy is now applied to the noise generated by the flow around a conventional helicopter rotor test case, described by Farassat [13]. The helicopter rotor consists of two equally spaced blades with 10 m in diameter and a constant chord of 0.4 m. The thickness ratio of the blades is 10% along the entire span of the blade. The blade tip Mach number is fixed at 0.6. The helicopter rotor operates at incidence with inflow Mach number of $M_\infty$ and angle of $\alpha$. The inflow angle is imposed by setting the uniform flow parallel to vector $(-\cos\alpha, 0, -\sin\alpha)$ as shown in Fig. 6. The free stream density $\rho_0$ and speed of sound $c_0$ are equal to 1.234 kg/m$^3$ and 340.75 m/s, respectively. The observer is located in the rotation plane at 50 m away from the rotation axis.

The blade surface is discretized into 75 cells around the blade airfoil and 100 divisions along the radial direction for the complete convergence. A non-uniform mesh density is used in both directions. The blade edges are an effective noise generation sources when the loading noise formula is studied numerically. Therefore, the grid points on the blade surface are clustered near the blade edges. The sources on the airfoil-shaped cut at the very tip and the inner radius of the blade are also taken into account. A calculation is performed for 128 time points per blade passage to resolve the pressure time history.

In order to analyze the Isom noise behavior against the angle of incidence, different angles of incidence are considered for the inflow Mach number of $M_\infty = 0.2$. Using the derived formulations, the acoustic pressure time history for the thickness and Isom source contributions is predicted. As shown in Fig. 10, the calculated Isom thickness noise and the monopole noise match quite well each other for different inflow angles. This agreement confirms that the derived

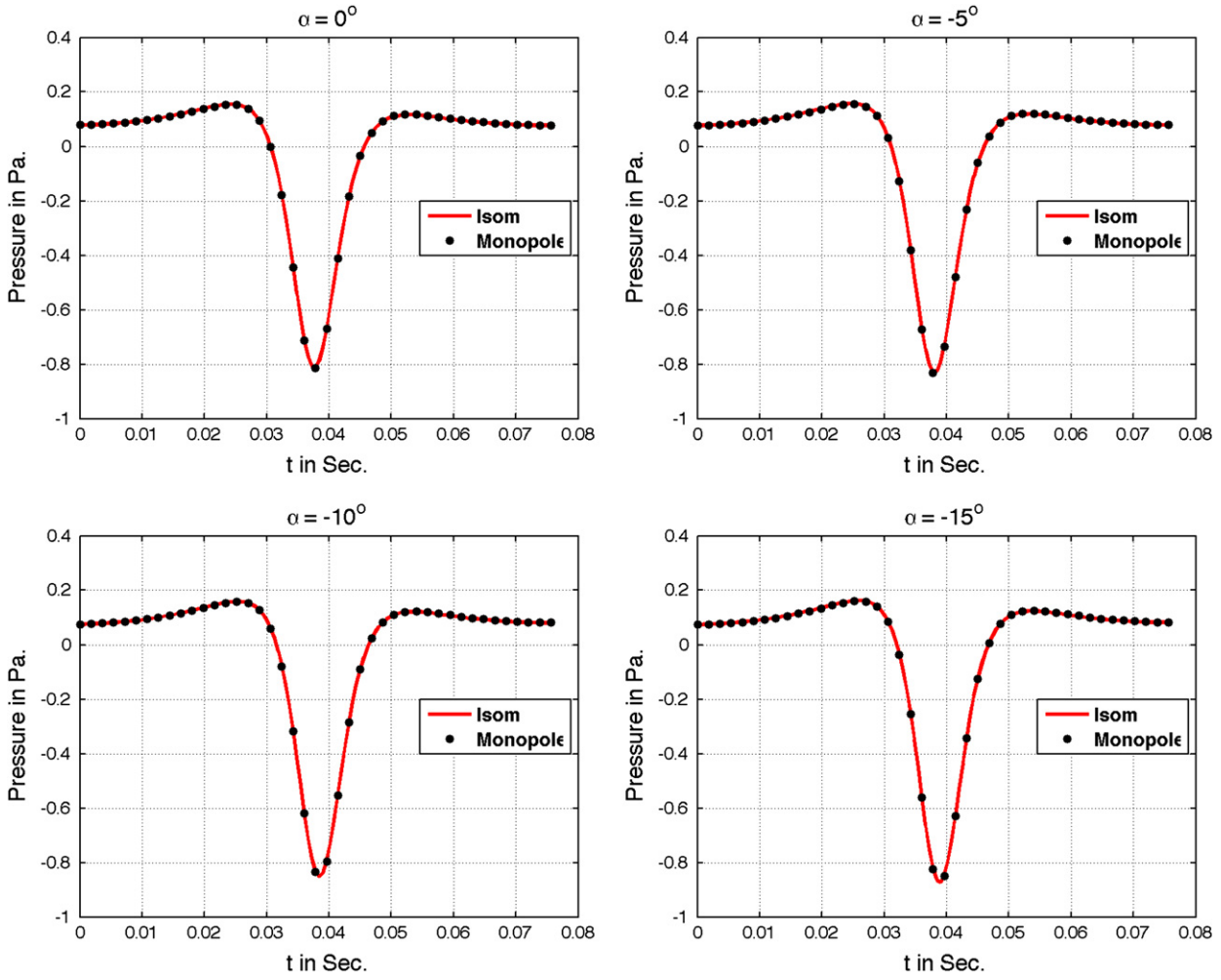


**Fig. 10.** Comparison between the calculated Isom thickness noise and computed monopole noise of the blades (NACA0010) with an inflow of $M_\infty = 0.2$. $M_{tip} = 0.6$ and $r = 50$ m.

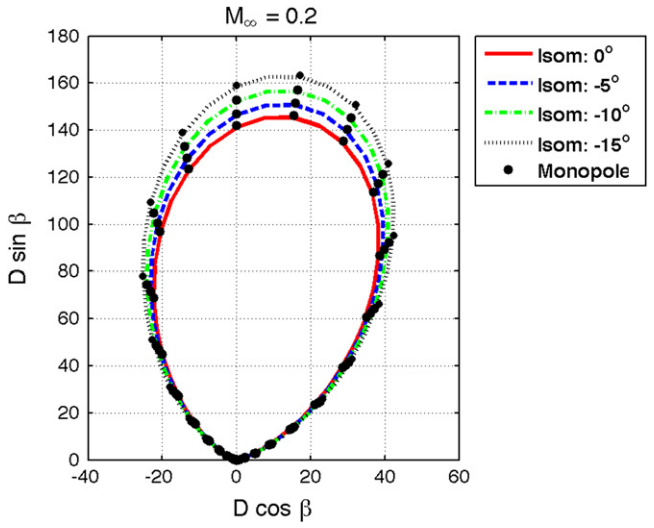


**Fig. 11.** The directivity of the predicted Isom thickness noise is shown for $M_\infty = 0.2$ and different inflow angles. $M_{tip} = 0.6$ and $r = 50$ m.

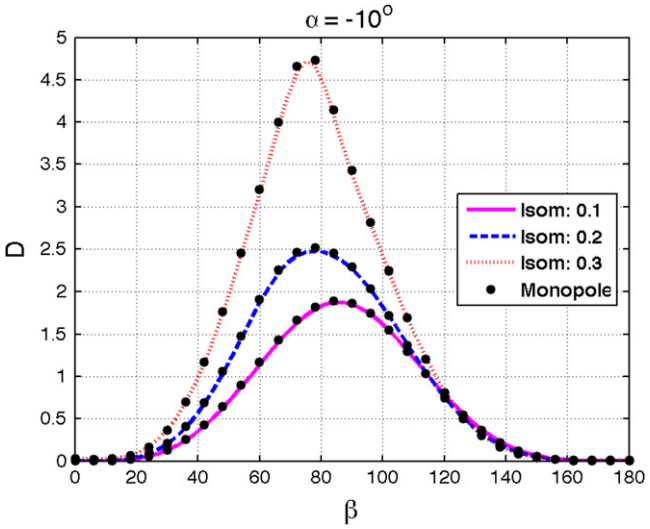


**Fig. 12.** Comparison of the directivity of the predicted Isom thickness noise with that of monopole noise is shown for $\alpha = -10^o$ and different inflow Mach numbers. $M_{tip} = 0.4$ and $r = 50$ m.

formulation can be used to accurately compute the acoustic pressure for a source case in a moving medium. It can be seen that due to increasing the inflow angle, the level of acoustic pressures increases.

For more investigation, the directivity of the acoustic pressure is also calculated. The observer is located at 50 m away from the rotation center and the angle defined by observer position vector and the rotation plane is varied. An angle of $90^o$ corresponds to the observer position at the rotation plane (see Fig. 2). Fig. 11 shows the calculated directivity for the blades operating at different angles of attack. As can be seen, the directivity feature shows a dipole pattern. In presence of the mean flow, acoustic pressures are maxima in the forward locations and minima along the rotation axis. A very good agreement between the Isom thickness noise directivity and the monopole noise directivity is also observed for all the inflow angles. It can be seen that by increasing the inflow angle the noise essentially increases everywhere.

In the next step, the Isom noise behavior of the rotating blades against the mean flow is evaluated. The blade tip Mach number is set to be 0.4. The angle of attack is kept at $\alpha = -10^o$ and the acoustic pressure time history is obtained for different inflow Mach numbers. Then, using the time history of the pressure fluctuations, the directivity of the acoustic pressure at each observer location is computed. Fig. 12 shows the calculated results for different inflow Mach numbers. It can be seen that due to the convective amplification, the level of acoustic pressures at a point in upstream is greater than the corresponding point in downstream. If the inflow Mach number increases the Doppler factor emphasizes the forward locations with the result that the forward noise increase is much more than the aft increase. The maximum value of the noise is also shifting to more forward locations. The excellent agreement between the thickness noise directivity and Isom noise directivity indicates that the derived formulation predicts the noise from sources in a moving medium accurately.

## 8. Conclusion

A detailed derivation of a linear acoustic time domain method for aerodynamic noise prediction that takes into account the mean flow effect was presented. An established theory of noise generation by a moving source was combined with a moving medium Green's function for derivation of the formulation. This Green's function is obtained by modification of that given by Blokhintsev. It was shown that the governing equation can be interpreted as a convective acoustic analogy equation and the solution generalizes that derived by Ffowcs Williams and Hawkings. It was also illustrated that the formulation developed can be interpreted as an extension of formulation 1 and 1A of Farassat to moving medium problems. The quality and ability of the formulation derived for cases in which the observer and the source are in motion with the same velocity in an arbitrary direction, and the source can also move relative to the observer were assessed through the five test cases.

Two analytical test cases, where a monopole point source and a dipole point source are positioned in a moving medium with arbitrary orientation, were modified and evaluated. Computations consisted of a permeable type data surface problem. A simple rotating point force in crossflow as a simple model of the acoustics of a propeller was the third test case. A consideration of this system has indicated the origin of the asymmetric noise field around a propeller at incidence. A model of helicopter blade, operating at incidence and described by Brentner was considered. This model was a case in which the thickness noise dominated the overall noise. The numerical technique was validated by comparison of the calculated thickness noise with that obtained with the NASA WOPWOP code.

Finally, a conventional helicopter blade was considered and the Isom thickness noise property was tested in the presence of mean flow with an arbitrary orientation. The Isom noise behavior of the rotating blades against the mean flow and the angle of incidence was analyzed. The numerical results were in excellent agreement between the results, indicating that developed formulation propagates the noise generated from of moving bodies in a moving medium accurately.

It is concluded that the derived formulation is useful and can be coded for efficient prediction of sound field generated by propellers at incidence.

## Acknowledgments

This research was funded by IWT under Project SBO 050163. This funding is gratefully acknowledged. The authors would also like to thank Dr. M. Carley of University of Bath for a valuable discussion.

## References

[1] J.E. Ffowcs Williams, D.L. Hawkings, Sound generation by turbulence and surfaces in arbitrary motion, *Philosophical Transactions of the Royal Society A* 264 (1151) (1969) 321–342.
[2] F. Farassat, Linear acoustic formulas for calculation of rotating blade noise, *AIAA Journal* 19 (9) (September 1981) 1122–1130.
[3] F. Farassat, G.P. Succi, The prediction of helicopter discrete frequency noise, *Veertica* 7 (4) (1983) 309–320.
[4] F. Farassat, Derivation of formulations 1 and 1A of Farassat, NASA, Technical Report TM 2007-2148 53, 2007.
[5] D.B. Hanson, Sound from a propeller at angle of attack: a new theoretical view point, *Proceedings: Mathematical and Physical Sciences* 449 (1936) (May 9, 1995) 315–325.
[6] D.B. Hanson, D.J. Paryzch, Theory for noise of propellers in angular inflow with parametric studies and experimental verification, USA, NASA Contractor's Report 4499, 1993.
[7] V.L. Wells, A.Y. Han, Acoustics of a moving source in a moving medium with application to propeller noise, *Journal of Sound and Vibration* 184 (4) (1995) 651–663.
[8] F. Farassat, Discontinuities in aerodynamics and aero-acoustics: the concept and application of generalized derivatives, *Journal of Sound and Vibration* 55 (2) (1977) 165–193.
[9] F. Farassat, Introduction to generalized functions with applications in aerodynamics and aeroacoustics, NASA Technical Paper TP 3428, 1996.
[10] D. Blokhintsev, Acoustics of a nonhomogeneous moving medium, NACA, Technical Report TM-1399, 1956.
[11] M. Carley, J.A. Fitzpatrick, Linar acoustic formulae for calculation of rotationg blade noise with asymmetric inflow, *CEAS/AIAA Conference*, *AIAA 96-1789*, 1996.
[12] F. Farassat, Extension of Isom's Thickness Noise Formula to the Near Field, *Journal of Sound and Vibration* 67 (22) (1979) 280–281.
[13] F. Farassat, Isom thickness noise formula for rotating blades with finite thickness at the tip, *Journal of Sound and Vibration* 72 (October 1980) 550–553.
[14] A.P. Dowling, J.E. Ffowcs Williams, *Sound and Sources of Sound*, Horwood Publishing, Westergate, 1983, pp. 207–208.
[15] S.W. Rienstra, A. Hirschberg, *An Introduction to Acoustics*, Eindhoven University of Technology, 2006.
[16] K.S. Brentner, Prediction of helicopter rotor discrete frequency noise, NASA, Technical Memorandum, 1986.
[17] K.S. Brentner, F. Farassat, Modeling aerodynamically generated sound of helicopter rotors, *Progress in Aerospace Sciences* 39 (2) (February 2003) 83–120.
[18] G. Ghorbaniasl, Ch. Hirsch, Validation of a time domain formulation for propeller noise prediction, *International Journal of Aeroacoustics* 5 (4) (2006) 295–301.